Electronic Supplementary Material (ESI) for Materials Chemistry Frontiers.

Electronic Supplementary Information

High-Efficiency and Stable Red to Near-Infrared Organic Light-emitting Diodes Using Dinuclear Platinum(II) Complexes

Lian Wang[#], Zhenhua Wen[#], Yulin Xu, Youming Zhang, Jingsheng Miao, Zhanxiang Chen and Kai Li**

Shenzhen Key Laboratory of New Information Display and Storage Materials, College of Materials Science and Engineering, Shenzhen University, Shenzhen 518055, P. R. China

E-mail: zhangym@szu.edu.cn; kaili@szu.edu.cn

[#]These authors contributed equally to this work.

General and Instruments

All chemicals and materials, unless otherwise stated, were commercially available and used as received without further purification. All solvents for reactions and photophysical studies were of HPLC grade. ^{1}H Nuclear magnetic resonance (NMR) spectra were recorded on a Bruker DRX 400 spectrometer using tetramethyl silane as an internal reference in deuterated chloroform solution at 298 K. High-resolution mass spectrometric measurements were performed on an Aglient 6550 spectrometer. Elemental analysis (EA) was performed on Elemantar: Vario EL cube lemantar. Thermogravimetric analysis (TGA) was conducted under a dry nitrogen gas flow at a heating rate of 10 ^{o}C min^{-1} on a Perkin- Elmer TGA 7. Shimadzu UV-2600 spectrophotometer (Shimadzu, Japan) was applied to record the UV-Vis spectra. Photoluminescence (PL) spectra were recorded on a Hitachi F-7100 fluorescence spectrophotometer (Hitachi, Japan). The transient PL decay curves were obtained by FluoTime 300 spectrometer (PicoQuant GmbH) with a Picosecond Pulsed UV-LASTER (LASTER485) as the excitation source. The photoluminescence quantum yields (PLQYs) were achieved by a Hamamatsu UV-NIR absolute PL quantum yield spectrometer (C13534, Hamamatsu Photonics) equipped with a calibrated integrating sphere. In the course of transient PL and PLQY measurements for thin films, the samples were exposed to dry argon to preclude the oxygen quenching effect. Thin doped PMMA and neat films for steady state and transient photoluminescence measurements were prepared by drop-casting of a solution followed by air-drying.

Single Crystal Analysis

Single crystals of all three complexes were obtained by layering methanol onto a DCM solution of each complex which undergoes slow diffusion. X-ray diffractions of all complexes were recorded on a Bruker D8 Venture diffractometer using MoKα radiation (λ = 0.71073 Å). The crystal was kept at 150.0 or 170.0 K during data collection. Using Olex2,[1] the structure was determined with the ShelXT[2] structure solution program using intrinsic phasing and refined with the ShelXL refinement package using least-squares minimization.[3] Full crystallographic information in CIF format has been deposited at the Cambridge Crystallographic Data Center (CCDC), which can be obtained free from the website of www.ccdc.cam.ac.un/conts/retrieving.html.

Device fabrication and characterization

For devices fabrications, the layers of ITO/HATCN (5 nm)/TAPC (30 nm)/TCTA (15 nm)/DMIC-Cz+DMIC-TRz: Pt(II) emitter (50 nm)/ANT-BIZ (30 nm)/Liq (2 nm)/Al (100 nm) were successively deposited on the pre-cleaned ITO glass substrates at a pressure of less than 10^{-4} Pa. Indium-tin-oxide (ITO) coated glass with a sheet resistance of 10 Ω/sq was used as the anode substrate. Before film deposition, patterned ITO substrates were cleaned with detergent, rinsed in de-ionized water, acetone, and isopropanol, and then dried in an oven for 1 h in a cleanroom. The slides were then treated in an ultraviolet-ozone chamber for 5 min. The active area of devices was 3 mm × 3 mm. The EL spectra of devices were measured by fiber optic spectrometer (Ocean Optics USB 2000) in the normal direction. The *J-V-L* or *R-V-L* curves were investigated

by a dual-channel Keithley 2614B source measure unit and a PIN-25D silicon photodiode. All the measurements were conducted at room temperature under ambient condition. For operational stability studies, the devices were encapsulated with glass lids by UV curing adhesive in a nitrogen-filled glove box and then taken out from the glove box for lifetime tests. The luminance of the working devices in the normal direction were measured using an OLED lifetime testing system (FS-MP64, Suzhou FSTAR Scientific Instrument Co., Ltd, China) under a constant current density.

Quantum Chemical Calculations

Quantum chemical calculations were performed using the Gaussian 09 program package[4], using the B3LYP functional[5], LANL2DZ[6] basis set for platinum, and 6-31G[8] for all other atoms. No solvent was applied to all calculations, and results were analyzed further with Gauss View. Time-dependent DFT (TD-DFT) calculations were also carried out by this method on the basis of optimized ground-state geometries. The RMSDs were calculated with the software of VMD by referring to the configuration of S_0. The SOCs between S_n and T_n (n = 1, 2) states were calculated with PySOC by considering that the three T_n substrates (m = 1, 0, -1) are degenerate, i.e., $\hat{H}$, where the $\hat{H}_{soc}$ represents the interaction of the SOC. All RMSDs and SOCs were obtained at the TD-DFT level of theory using the B3LYP functional and the 6-31G(d,p) basis set.

Table S1. Crystal data and structure refinement for complexes **Pt-1** ~ **Pt-4**.

Identification code	Pt-1	Pt-2	Pt-3	Pt-4
Empirical formula	$C_{44}H_{28}F_2N_6Pt_2$	$C_{42}H_{30}N_6Pt_2S_2$	$C_{42}H_{24}F_4N_8Pt_2$	$C_{52}H_{34}N_6Pt_2$
Formula weight	1068.90	1073.02	1106.87	1133.04
Temperature/K	170.0	150	170.0	150
Crystal system	tetragonal	monoclinic	triclinic	triclinic
Space group	$P4_3$	$P2_1/c$	P-1	P-1
a/Å	14.1699(3)	10.9057(6)	10.4675(4)	11.9473(9)
b/Å	14.1699(3)	29.2548(13)	14.3845(6)	12.5507(10)
c/Å	34.5036(10)	11.7171(6)	15.9689(7)	14.2057(11)
α/°	90	90	66.550(2)	99.063(3)
β/°	90	107.714(2)	77.958(2)	112.730(2)
γ/°	90	90	69.9680(10)	92.144(3)
Volume/Å^3	6927.8(4)	3561.0(3)	2065.09(15)	1928.8(3)
Z	8	4	2	4
ρ_{calc}g/cm^3	2.050	2.001	1.780	1.951
μ/mm^{-1}	8.123	8.007	6.824	7.293
F(000)	4064.0	2048.0	1048.0	1088.0
Crystal size/mm^3	0.18 × 0.06 × 0.05	0.15 × 0.08 × 0.05	0.45 × 0.38 × 0.1	0.15 × 0.06 × 0.04
Radiation	MoKα (λ = 0.71073)	MoKα (λ = 0.71073)	MoKα (λ = 0.71073)	MoKα (λ = 0.71073)
2Θ range for data collection/°	4.562 to 52.726	3.906 to 52.78	4.958 to 54.332	3.806 to 53.228
Index ranges	-15 ≤ h ≤ 17, -12 ≤ k ≤ 17, -42 ≤ l ≤ 41	-13 ≤ h ≤ 13, -36 ≤ k ≤ 35, -14 ≤ l ≤ 14	-12 ≤ h ≤ 13, -18 ≤ k ≤ 18, -20 ≤ l ≤ 20	-12 ≤ h ≤ 14, -15 ≤ k ≤ 15, -17 ≤ l ≤ 16
Reflections collected	35007	33538	49288	21589
Independent reflections	13868 [R_{int} = 0.0457, R_{sigma} = 0.0690]	7239 [R_{int} = 0.0901, R_{sigma} = 0.0771]	9149 [R_{int} = 0.0507, R_{sigma} = 0.0381]	7918 [R_{int} = 0.0611, R_{sigma} = 0.0826]
Data/restraints/parameters	13868/2099/973	7239/0/471	9149/0/505	7918/18/541
Goodness-of-fit on F^2	0.990	1.027	1.048	1.026
Final R indexes [I>=2σ (I)]	R_1 = 0.0377, wR_2 = 0.0624	R_1 = 0.0424, wR_2 = 0.0710	R_1 = 0.0308, wR_2 = 0.0912	R_1 = 0.0491, wR_2 = 0.0881
Final R indexes [all data]	R_1 = 0.0570, wR_2 = 0.0722	R_1 = 0.0748, wR_2 = 0.0834	R_1 = 0.0359, wR_2 = 0.0943	R_1 = 0.0886, wR_2 = 0.1032
Largest diff. peak/hole / e Å^{-3}	0.76/-0.53	1.05/-1.64	1.30/-1.82	1.79/-1.68
CCDC No.	2209083	2209084	2209085	2209086

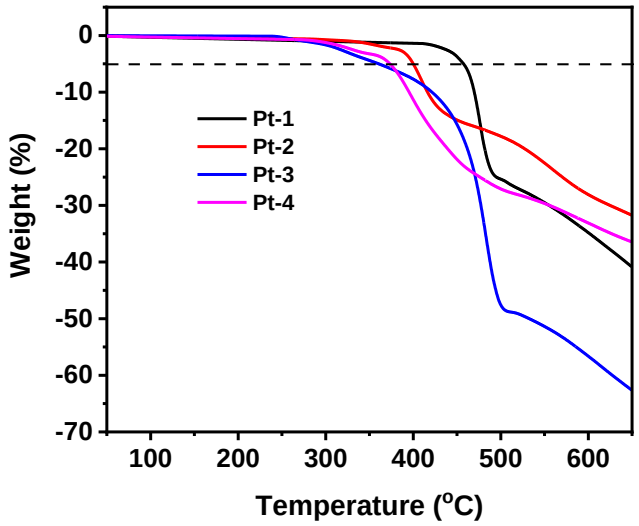

Figure S1. Thermogravimetric analysis curves for **Pt-1**, **Pt-2**, **Pt-3**, and **Pt-4**.

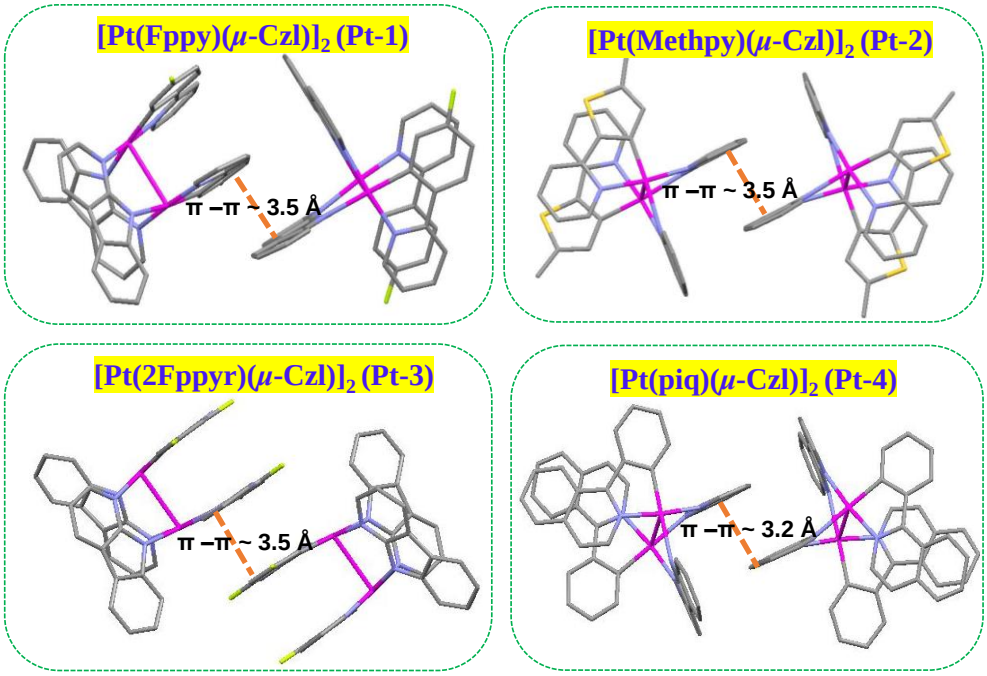

Figure S2. Packing mode of **Pt-1**, **Pt-2**, **Pt-3**, and **Pt-4** in the crystal structures.

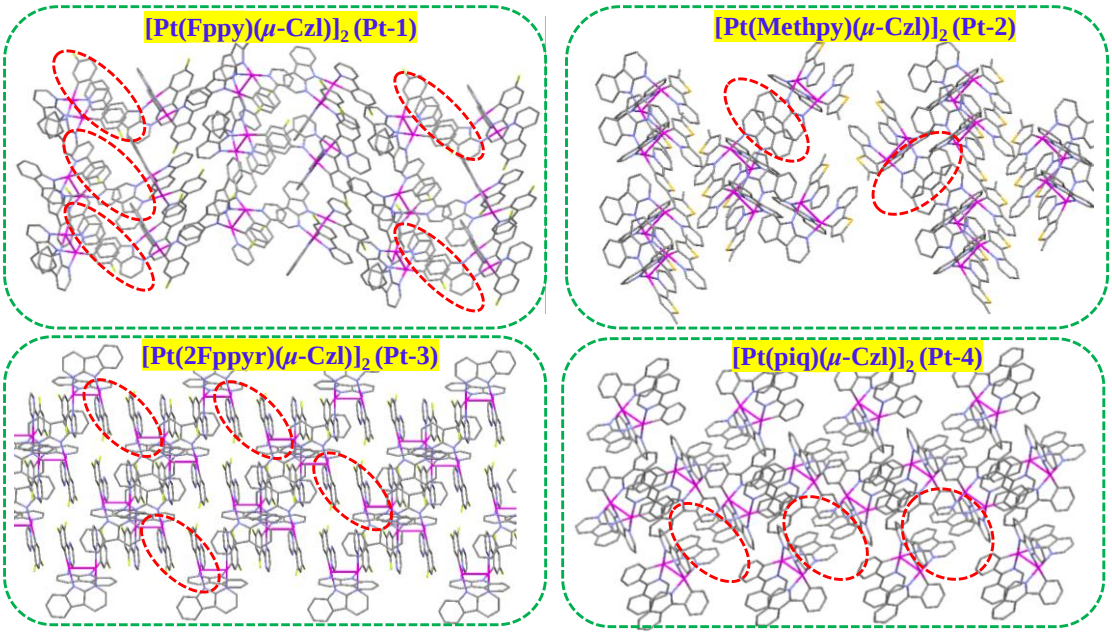

Figure S3. Packing mode of **Pt-1**, **Pt-2**, **Pt-3**, and **Pt-4** in the crystal structures.

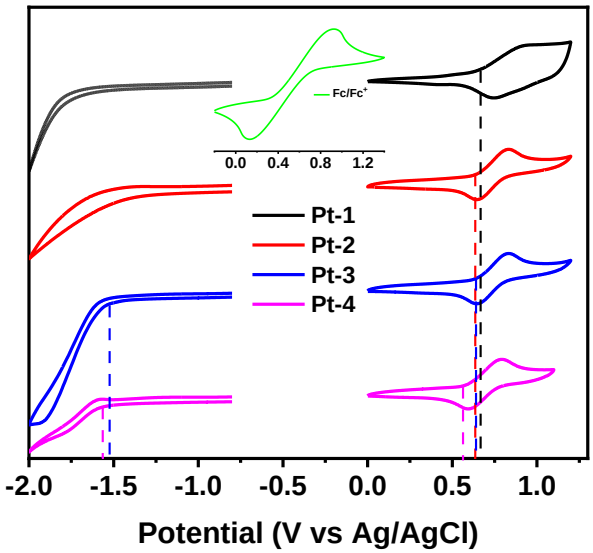

Figure S4. Cyclic voltammograms for **Pt-1**, **Pt-2**, **Pt-3**, and **Pt-4** in DCM solution with a scan rate of 100 mV s^{-1} using 0.1 mol/L Bu_4NPF_6 and ferrocene as the electrolyte and internal standard, respectively.

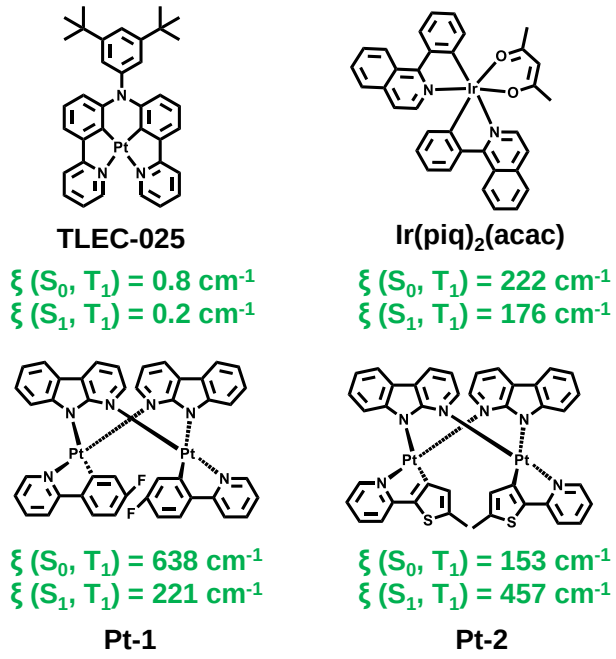

Figure S5. Molecular structures and the SOC constants of reported Pt(II) (**TLEC-025**; *Adv. Mater*. **2012**, *24*, 5099-5103) and Ir(III) (**Ir(piq)2(acac)**; *Adv. Mater.* **2003**, *15*, 884-888) complexes, as well as **Pt-1** and **Pt-2** in this work.

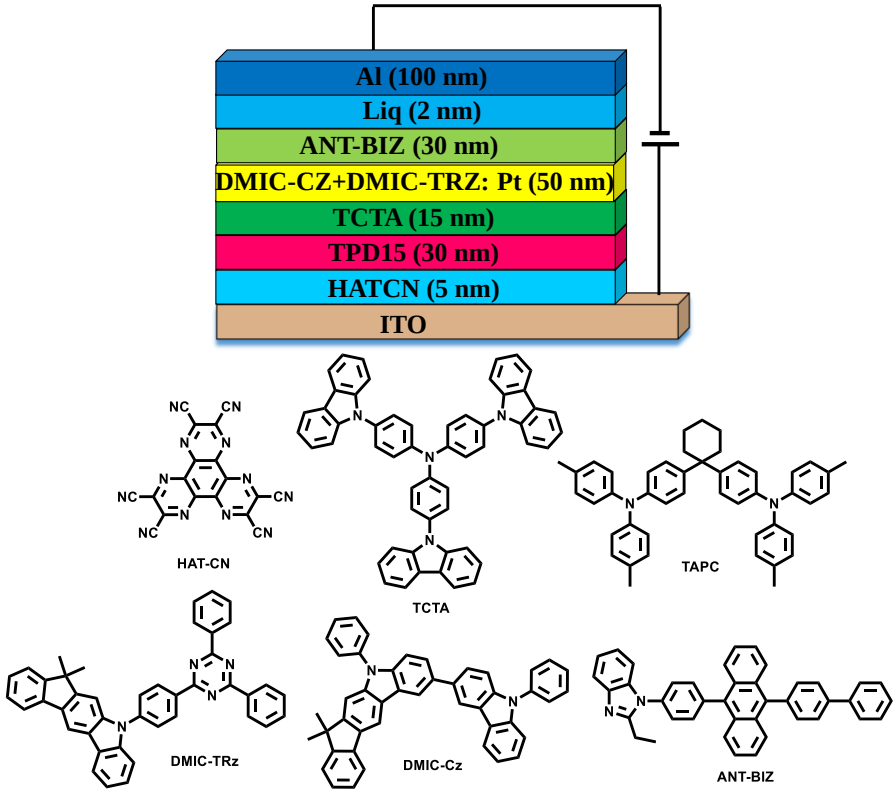

Figure S6. Device configuration and chemical structures of HAT-CN, TCTA, TAPC, DMIC-Cz, DMIC-TRz and ANTBIZ.

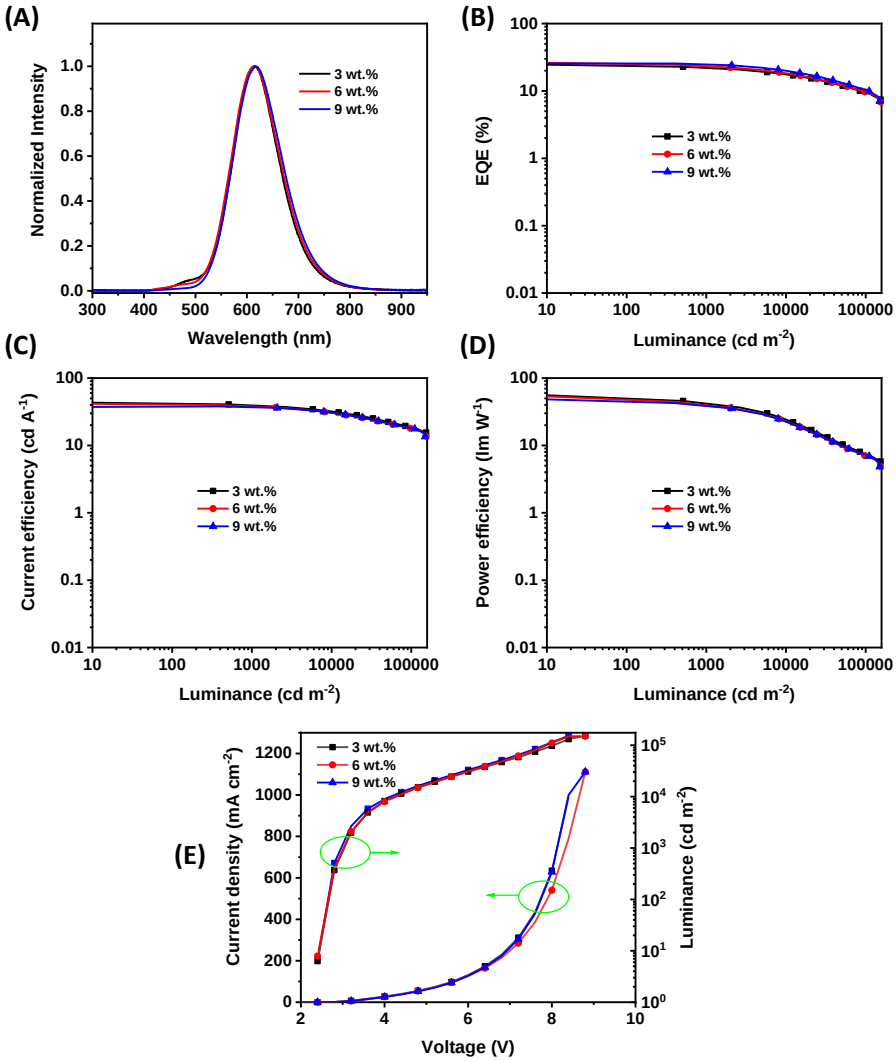

Figure S7. (A) Normalized EL spectra, (B) EQE-luminance characteristics, (C) CE-luminance characteristics, (D) PE-luminance characteristics and (E) *J-V-L* characteristics of OLEDs with **Pt-1** as the emitter.

Table S2. Key performances of OLEDs based on **Pt-1** as the emitter.

Pt-1	λ *(nm)*	L^a_{max} (cd m^{-2})	*CE*^{b} *(*cd A^{-1}*)*	*PE*^{c} *(*lm W^{-1}*)*	*EQE*^{d} *(%)*	*CIE*^{e} (x, y)
3 wt.%	615	153370	43.4/39.3	56.8/41.8	24.7/22.0	0.58, 0.42
6 wt.%	615	153065	41.7/38.0	54.6/39.4	26.4/23.3	0.59, 0.41
9 wt.%	617	149815	37.9/37.0	48.4/38.4	25.6/24.7	0.60, 0.40

(a) Maximum luminance. (b) The maximun current efficiency (left) and the value at 1000 cd m^{-2} (right). (c) The maximum power efficiency (left) and the value at 1000 cd m^{-2} (right). (d) The maximun external quantum efficiency (left) and the value at 1000 cd m^{-2} (right). (e) CIE coordinates @EQE$_{max}$.

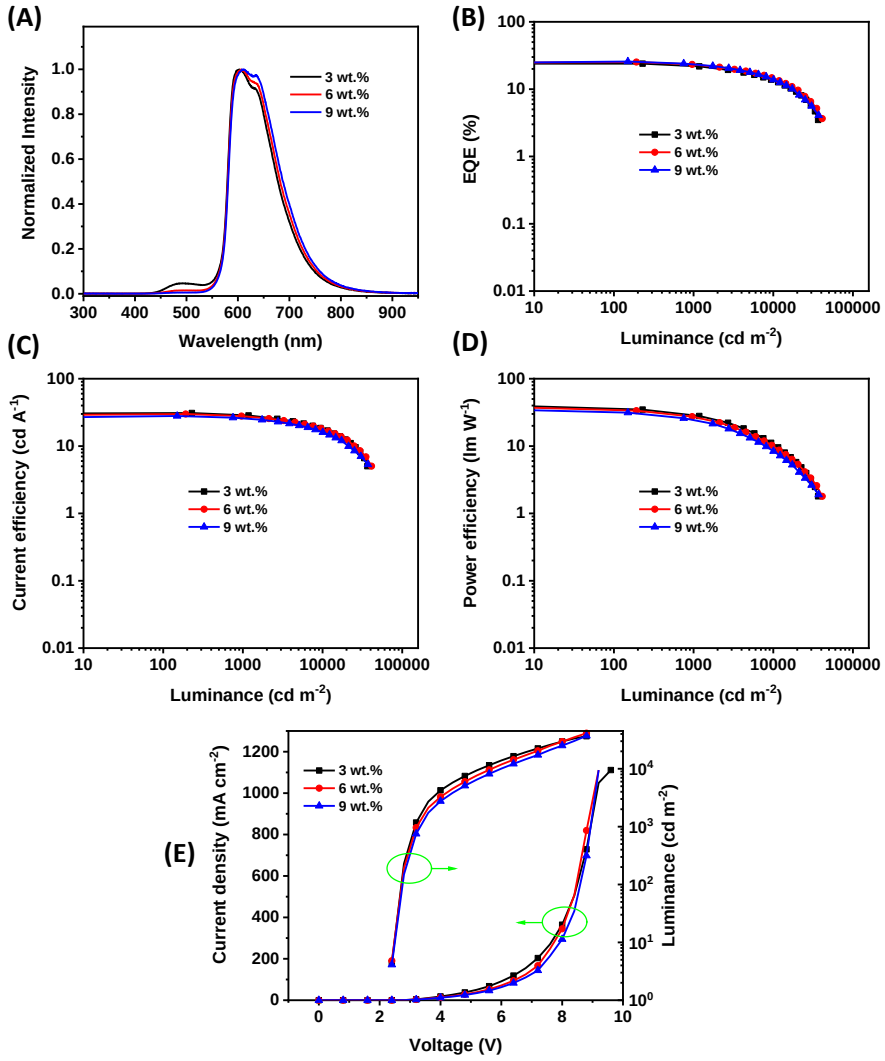

Figure S8. (A) Normalized EL spectra, (B) EQE-luminance characteristics, (C) CE-luminance characteristics, (D) PE-luminance characteristics and (E) *J-V-L* characteristics of OLEDs with **Pt-2** as the emitter.

Table S3. Key performances of OLEDs based on **Pt-2** as the emitter.

Pt-2	λ *(nm)*	L^a_{max} (cd m^{-2})	*CE*^{b} *(*cd A^{-1}*)*	*PE*^{c} *(*lm W^{-1}*)*	*EQE*^{d} *(%)*	*CIE*^{e} (x, y)
3 wt.%	602/633	36556	31.0/28.0	39.9/28.6	23.9/22.0	0.63, 0.37
6 wt.%	606/635	41191	30.0/27.8	33.6/27.2	25.2/23.2	0.64, 0.34
9 wt.%	610/635	37142	27.9/25.8	34.9/24.4	25.7/23.4	0.64, 0.36

(a) Maximum luminance. (b) The maximun current efficiency (left) and the value at 1000 cd m^{-2} (right). (c) The maximum power efficiency (left) and the value at 1000 cd m^{-2} (right). (d) The maximun external quantum efficiency (left) and the value at 1000 cd m^{-2} (right). (e) CIE coordinates @EQE$_{max}$.

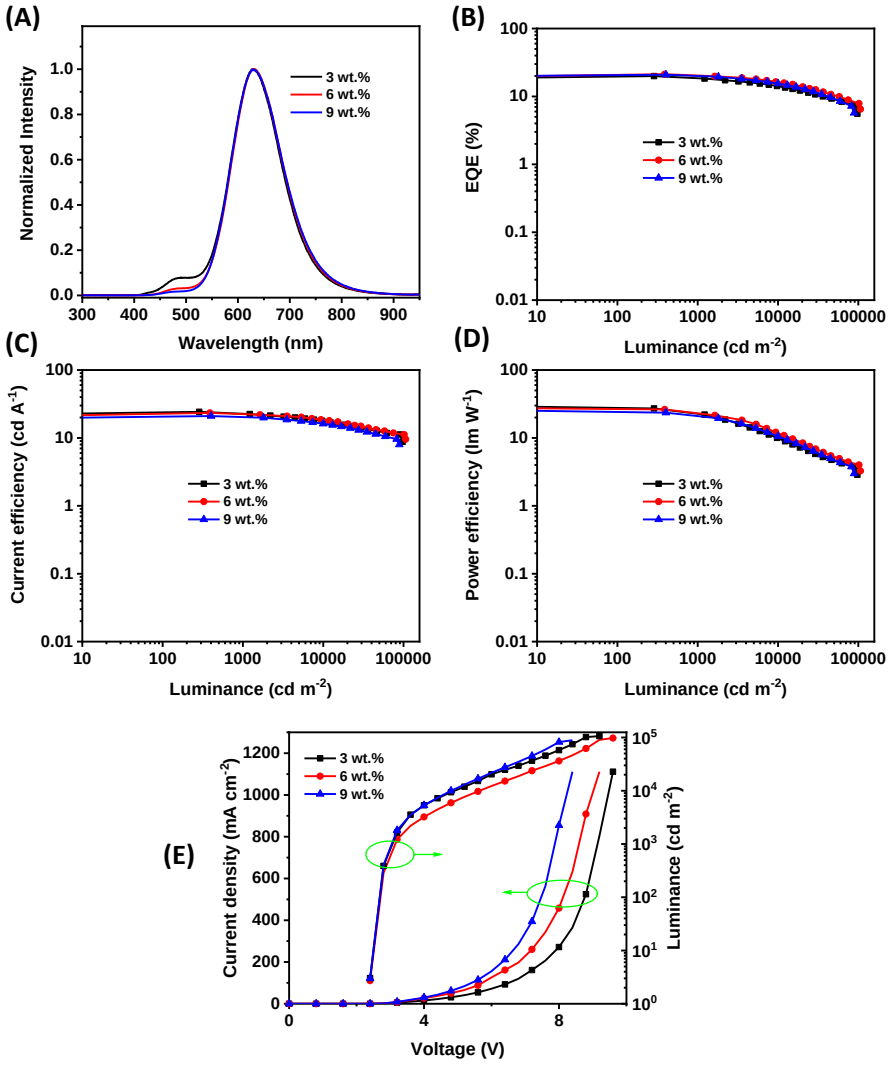

Figure S9. (A) Normalized EL spectra, (B) EQE-luminance characteristics, (C) CE-luminance characteristics, (D) PE-luminance characteristics and (E) *J-V-L* characteristics of OLEDs with **Pt-3** as the emitter.

Table S4. Key performances of OLEDs based on **Pt-3** as the emitter.

Pt-3	λ *(nm)*	L^a_{max} (cd m^{-2})	*CE*^{b} *(*cd A^{-1}*)*	*PE*^{c} *(*lm W^{-1}*)*	*EQE*^{d} *(%)*	*CIE*^{e} (x, y)
3 wt.%	630	97312	24.2/22.1	29.3/22.7	19.9/18.5	0.60, 0.38
6 wt.%	630	106231	23.4/22.4	27.6/23.0	21.3/20.3	0.62, 0.38
9 wt.%	630	88673	21.0/20.2	25.6/20.9	20.9/20.0	0.64, 0.36

(a) Maximum luminance. (b) The maximun current efficiency (left) and the value at 1000 cd m^{-2} (right). (c) The maximum power efficiency (left) and the value at 1000 cd m^{-2} (right). (d) The maximun external quantum efficiency (left) and the value at 1000 cd m^{-2} (right). (e) CIE coordinates @EQE$_{max}$.

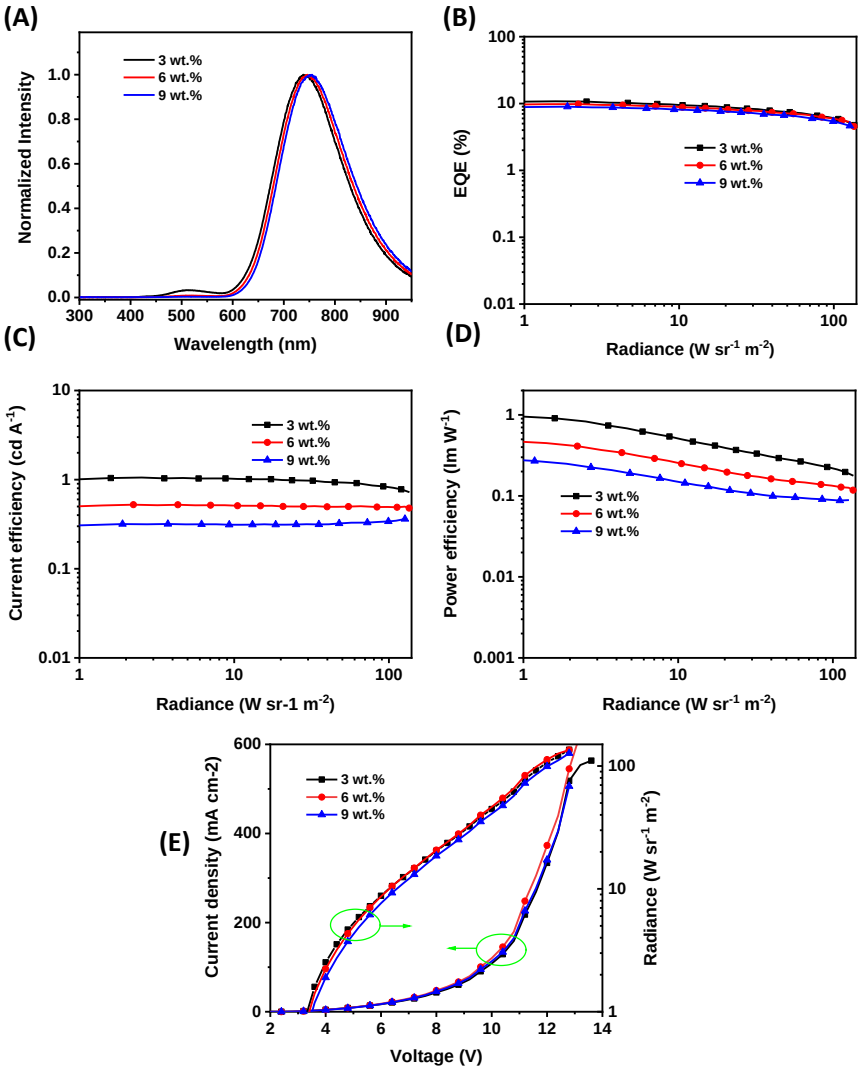

Figure S10. (A) Normalized EL spectra, (B) EQE-radiance characteristics, (C) CE- radiance characteristics, (D) PE- radiance characteristics and (E) *J-V-R* characteristics of OLEDs with **Pt-4** as the emitter.

Table S5. Key performances of OLEDs based on **Pt-4** as the emitter.

Pt-3	λ *(nm)*	R^{a}_{max} (W sr^{-1} m^{-2})	CE^{b} *(*cd A^{-1}*)*	PE^{c} *(*lm W^{-1}*)*	EQE^{d} *(%)*	CIE^{e} (x, y)
3 wt.%	740	136	1.0/1.0	1.0/0.5	10.8/9.5	0.66, 0.36
6 wt.%	746	135	0.5/0.5	0.5/0.3	9.8/8.8	0.67, 0.32
9 wt.%	755	127	0.4/0.3	0.5/0.1	9.0/8.1	0.69, 0.30

(a) Maximum radiance. (b) The maximun current efficiency (left) and the value at 10000 mW sr^{-1} m^{-2} (right). (c) The maximum power efficiency (left) and the value at 10000 mW sr^{-1} m^{-2} (right). (d) The maximun external quantum efficiency (left) and the value at 10000 mW sr^{-1} m^{-2} (right). (e) CIE coordinates @EQE$_{max}$.

Table S6. Device data of red and NIR doped OLEDs based on selected representative emitters in the literature and comparison with this work.

Device type	Category	Emitters	$\lambda_{EL,max}$ [nm]	EQE_{Max} [%]	*Ref.*
Vacuum evaporation	[Pt(II)]	**Pt-1**	615	26.4	This work
Vacuum evaporation	[Pt(II)]	**Pt-2**	610/635	25.7	This work
Vacuum evaporation	[Pt(II)]	**Pt-3**	630	21.3	This work
Vacuum evaporation	[Pt(II)]	**Pt-4**	740	10.8	This work
		Red OLEDs			
Vacuum evaporation	[Pt(II)]	**1**	639	23.3	8
Vacuum evaporation	[Pt(II)]	**2**	625	21.0	8
Vacuum evaporation	[Pt(II)]	**PtN3N-ptb**	606	21.5	9
Vacuum evaporation	[Pt(II)]	**TLEC-025**	620	19.5	10
Vacuum evaporation	[Pt(II)]	**$Pt2L(acac)_2$**	612	9.9	11
Vacuum evaporation	[Pt(II)]	**Pt-4**	610	11.7	12
Solution-processed	[Pt(II)]	**Pt-5**	607	7.4	13
Vacuum evaporation	[Os(II)]	**$Os(fptz)_2(PPh_2Me)_2$**	616	19.9	14
Vacuum evaporation	[Rh(III)]	**Rh-3**	600	12.2	15
Solution-processed	[Au(III)]	**Au-2**	636	3.6	16
Solution-processed	[Au(III)]	**Au5**	616	5.3	17
		NIR OLEDs			
Vacuum evaporation	[Pt(II)]	**3**	725	15.0	8
Solution-processed	[Pt(II)]	**$(2niq)_2Pt_2(u\text{-}OXT)_2$**	704	8.9	18
Solution-processed	[Pt(II)]	**$(piq)Pt(u\text{-}OXT)_2Pt(piq)$**	706	6.3	19
Vacuum evaporation	[Pt(II)]	**PtPor**	769	6.3	20
Vacuum evaporation	[Pt(II)]	**PtPor2**	773	9.2	21
Vacuum evaporation	[Os(II)]	**$[Os(ftrmpz)_2(PPhMe)_2]$**	710	11.5	22
Vacuum evaporation	[Os(II)]	**Os-4**	718	2.7	23
Vacuum evaporation	[Os(II)]	**Os-1**	814	1.5	23

Solution-processed	[Ir(III)]	**Ir3**	708	13.7	24
Solution-processed	[Pt(II)]	**DPTAIr**	800	2.98	25
Vacuum evaporation	[Ir(III)]	***fac*-Ir(Ftbpa)$_3$**	760	4.5	26
Solution-processed	[Au(III)]	**1b**	720	0.2	27
Vacuum evaporation	TADF	**TPA-PZTCN**	734	13.4	28
Vacuum evaporation	TADF	**DCPA-TPA**	838	0.58	29

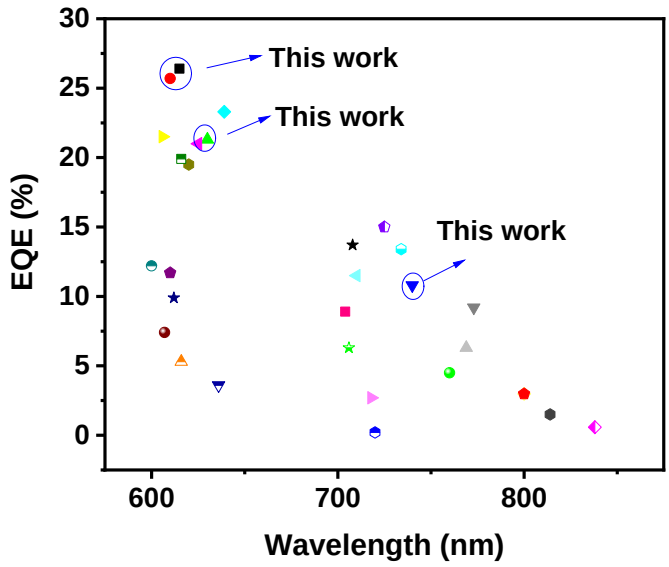

Figure S11. Maximum EQE versus the emission wavelength of red and NIR emitters presented in Table S6.

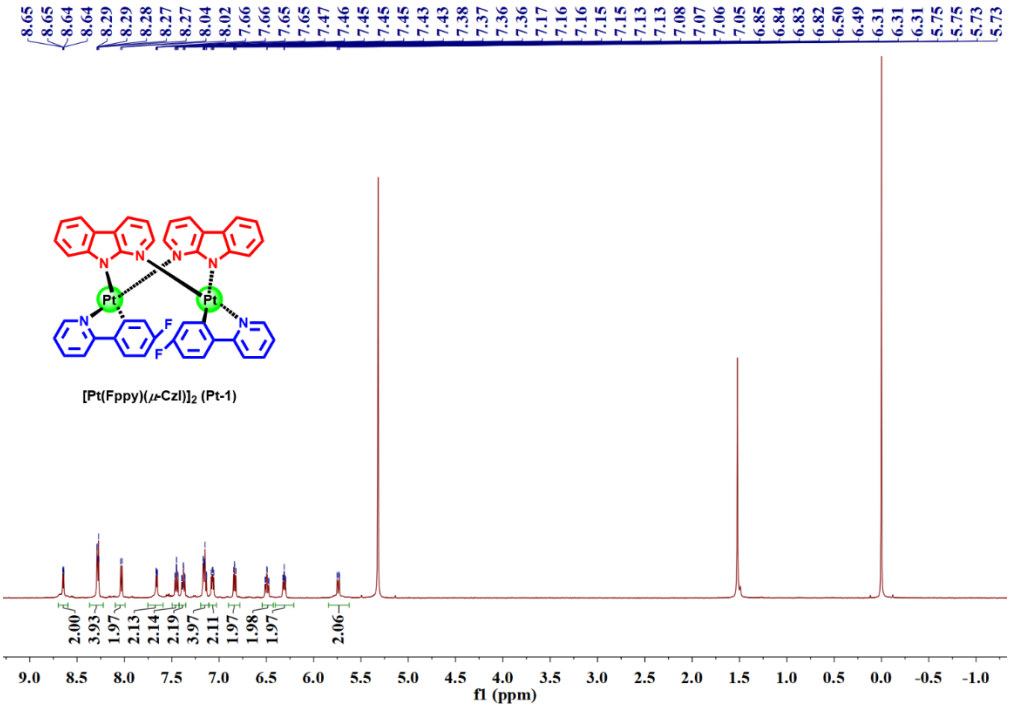

Figure S12. ^{1}H NMR spectrum of **Pt-1**.

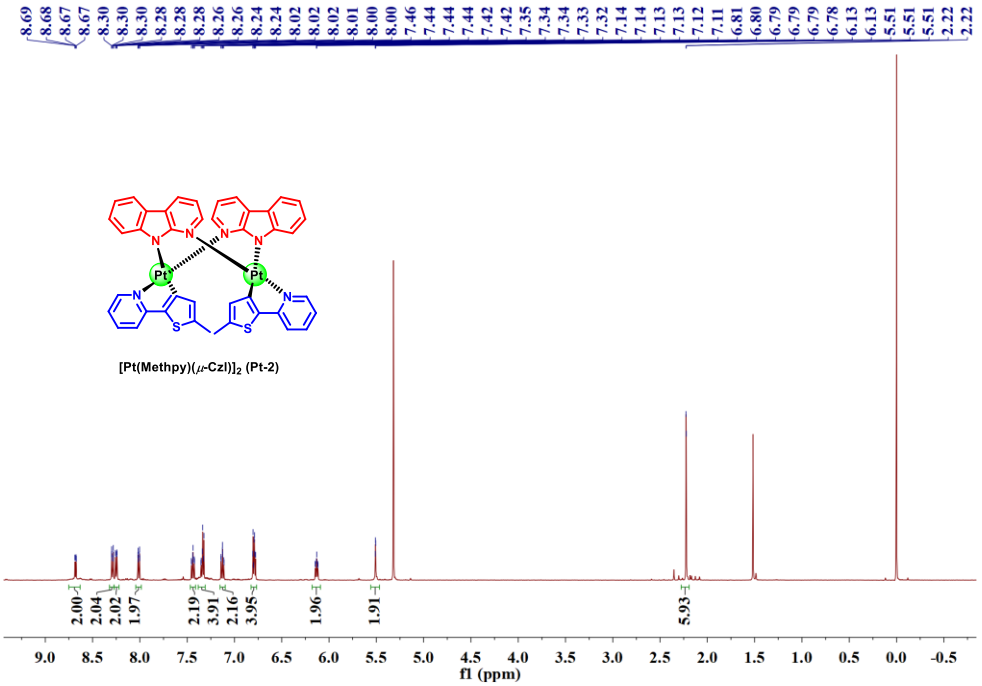

Figure S13. ^{1}H NMR spectrum of **Pt-2**.

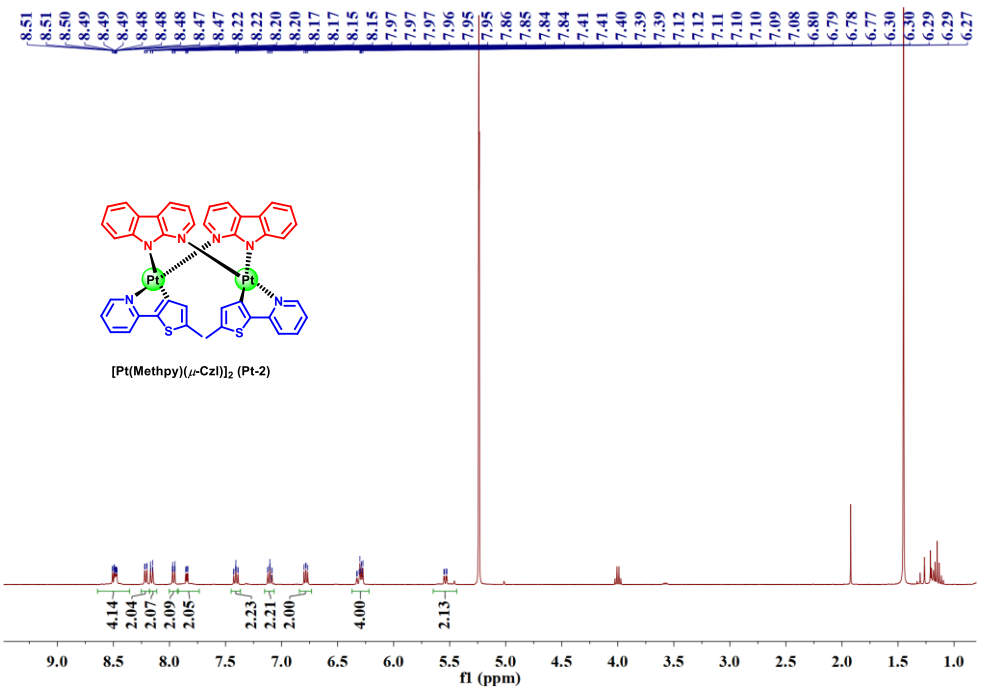

Figure S14. ^{1}H NMR spectrum of **Pt-3**.

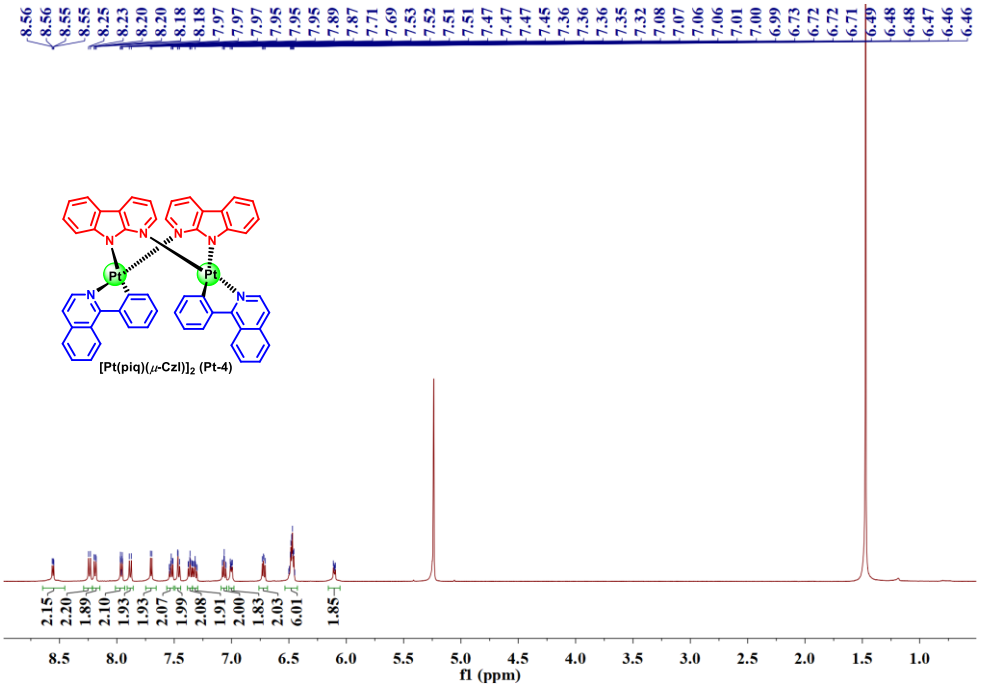

Figure S15. ^{1}H NMR spectrum of **Pt-4**.

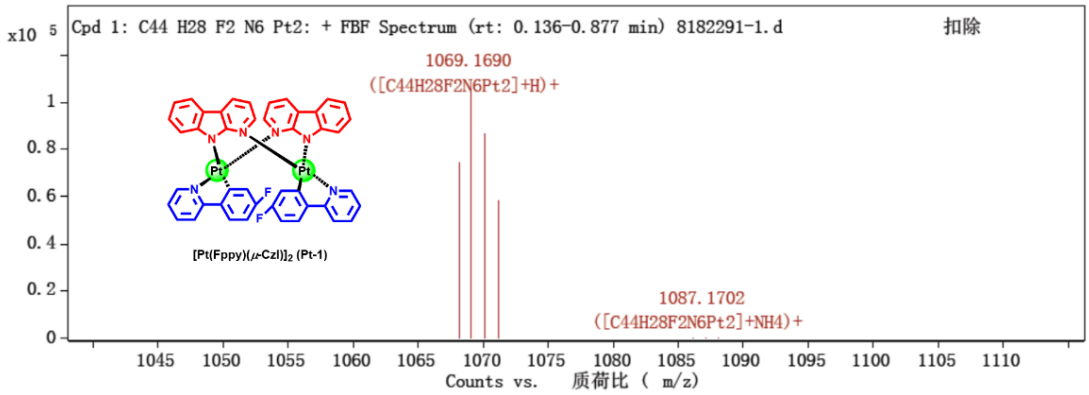

Figure S16. HRMS spectrum of **Pt-1**.

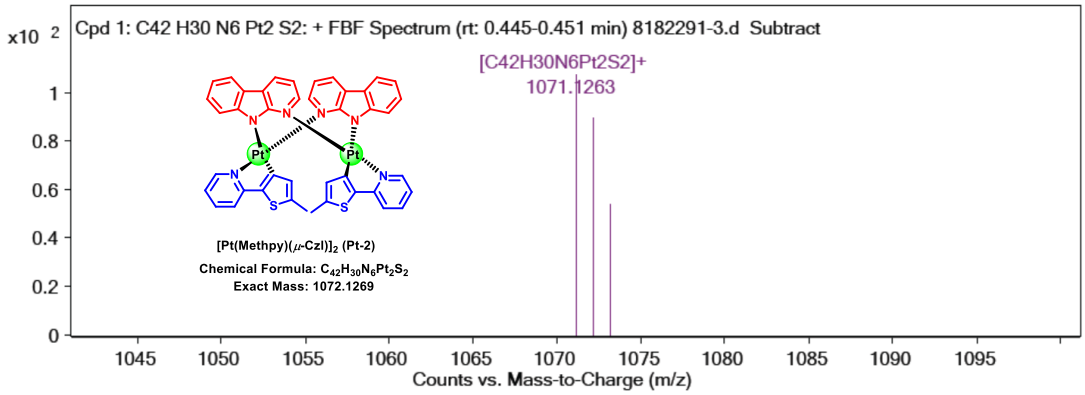

Figure S17. HRMS spectrum of **Pt-2**.

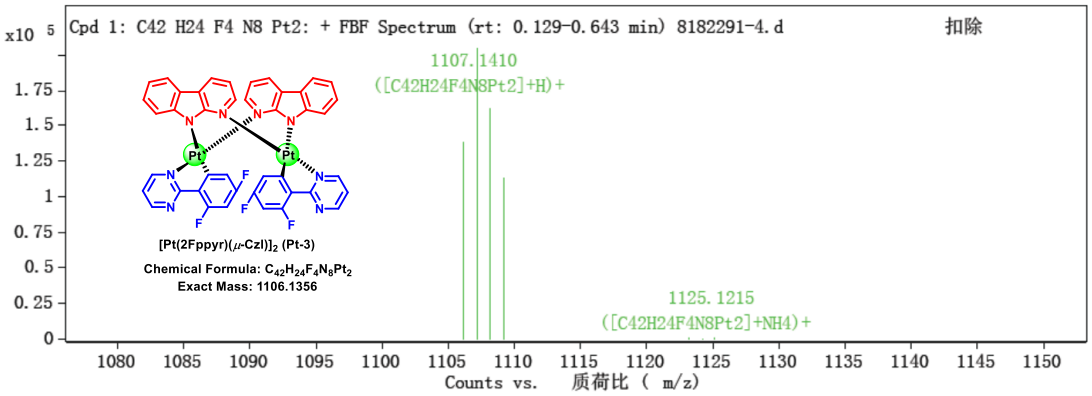

Figure S18. HRMS spectrum of **Pt-3**.

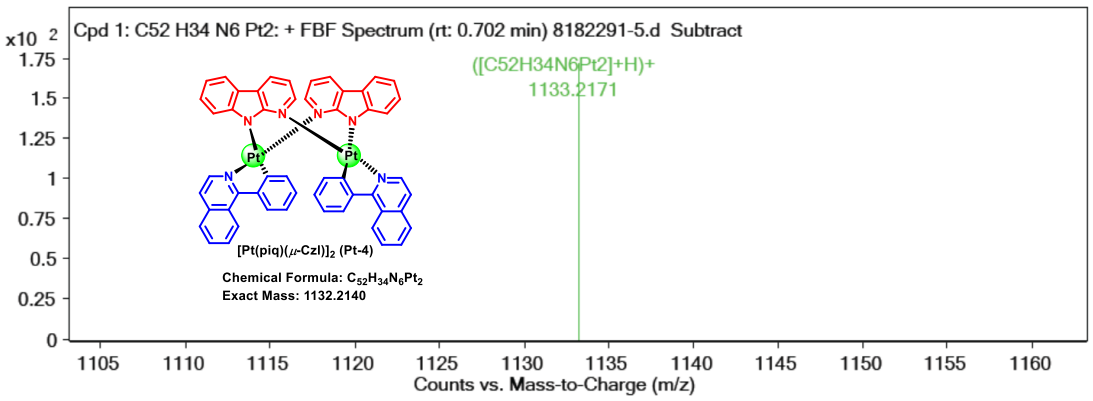

Figure S19. HRMS spectrum of **Pt-4**.

References

[1]. O. V. Dolomanov, L. J. Bourhis, R. J. Gildea, J. A. K. Howard, H. Puschmann, *J. Appl. Cryst.* **2009**, *42*, 339-341.

[2]. G. M. Sheldrick, *Acta. Cryst.* **2015**, *A71*, 3-8.

[3]. G. M. Sheldrick, *Acta. Cryst.* **2015**, *C71*, 3-8.

[4]. M. J. Frisch, G. W. Trucks, H. B. Schlegel, G. E. Scuseria, M. A. Robb, J. R. Cheeseman, G. Scalmani, V. Barone, B. Mennucci, G. A. Petersson, H. Nakatsuji, M. Caricato, X. Li, H. P. Hratchian, A. F. Izmaylov, J. Bloino, G. Zheng, J. L. Sonnenberg, M. Hada, M. Ehara, K. Toyota, R. Fukuda, J. Hasegawa, M. Ishida, T. Nakajima, Y. Honda, O. Kitao, H. Nakai, T. Vreven, J. A. Montgomery Jr, J. E. Peralta, F. Ogliaro, M. Bearpark, J. J. Heyd, E. Brothers, K. N. Kudin, V. N. Staroverov, R. Kobayashi, J. Normand, K. Raghavachari, A. Rendell, J. C. Burant, S. S. Iyengar, J. Tomasi, M. Cossi, N. Rega, J. M. Millam, M. Klene, J. E. Knox, J. B. Cross, V. Bakken, C. Adamo, J. Jaramillo, R. Gomperts, R. E. Stratmann, O. Yazyev, A. J. Austin, R. Cammi, C. Pomelli, J. W. Ochterski, R. L. Martin, K. Morokuma, V. G. Zakrzewski, G. A. Voth, P. Salvador, J. J. Dannenberg, S. Dapprich, A. D. Daniels, Ö . Farkas, J. B. Foresman, J. V. Ortiz, J. Cioslowski, D. J. Fox, Revision D.01 ed., Gaussian, Inc., Wallingford CT, **2009**.

[5]. a) A. D. Becke, *J. Chem. Phys*. **1993**, *98*, 5648; b) P. J. Stephens, F. J. Devlin, C. F. Chabalowski, M. J. Frisch, *J. Phys. Chem*. **1994**, *98*, 11623.

[6]. P. J. Hay, W. R. Wadt, *J. Chem. Phys*. **1985**, *82*, 299.

[7]. G. A. Petersson, M. A. Al Laham, *J. Chem. Phys*. **1991**, *94*, 6081.

[8]. Y. Zhang, J. Miao, J. Xiong, K. Li, C. Yang, *Angew. Chem. Int. Ed*. 2022, *61*, e202113718.

[9]. T. Fleetham, G. Li, J. Li, *ACS Appl. Mater. Interfaces* **2015**, *7*, 16240-16246.

[10]. H. Fukagawa, T. Shimizu, H. Hanashima, Y. Osada, M. Suzuki, H. Fujikake, *Adv. Mater.* **2012**, *24*, 5099-5103.

[11]. M. Z. Shafikov, R. Daniels, P. Pander, F. B. Dias, J. A. G. Williams, V. N. Kozhevnikov, *ACS Appl. Mater. Interfaces* **2019**, *11*, 8182-8193.

[12]. L. Zhou, C. L. Kwong, C. C. Kwok, G. Cheng, H. Zhang, C. M. Che, *Chem. Asian J.* **2014**, *9*, 2984-2994.

[13]. P. Pander, R. Daniels, A. V. Zaytsev, A. Horn, A. Sil, T. J. Penfold, J. A. G. Williams, V. N. Kozhevnikov, F. B. Dias, *Chem. Sci.* **2021**, *12*, 6172-6180.

[14]. C. H. Chien, F. M. Hsu, C. F. Shu, Y. Chi, *Org. Electron.* **2009**, *10*, 871-876.

[15]. F. Wei, S. L. Lai, S. Zhao, M. Ng, M. Y. Chan, V. W. Yam, K. M. Wong, *J. Am. Chem. Soc.* **2019**, *141*, 12863-12871.

[16]. M. C. Tang, C. K. M. Chan, D. P. K. Tsang, Y. C. Wong, M. M. Y. Chan, K. M. C. Wong, V. W. W. Yam, *Chem. Eur. J.* **2014**, *20*, 15233-15241.

[17]. C. C. Au Yeung, L. K. Li, M. C. Tang, S. L. Lai, W. L. Cheung, M. Ng, M. Y. Chan, V. W. W. Yam, *Chem. Sci.* **2021**, *12*, 9516-9527.

[18]. W. Xiong, F. Meng, C. You, P. Wang, J. Yu, X. Wu, Y. Pei, W. Zhu, Y. Wang, S. Su, *J. Mater. Chem. C* **2019**, *7*, 630-638.

[19]. X. Wu, Y. Liu, Y. Wang, L. Wang, H. Tan, M. Zhu, W. Zhu, Y. Cao, *Org. Electron.* **2012**, *13*, 932-937.

[20]. C. Borek, K. Hanson, P. I. Djurovich, M. E. Thompson, K. Aznavour, R. Bau, Y. Sun, S. R. Forrest, J. Brooks, L. Michalski, J. Brown, *Angew. Chem. Int. Ed.* **2007**, *46*, 1109-1112.

[21]. K. R. Graham, Y. Yang, J. R. Sommer, A. H. Shelton, K. S. Schanze, J. Xue, J. R. Reynolds, *Chem. Mater.* **2011**, *23*, 5305-5312.

[22]. Y. Yuan, J. L. Liao, S. F. Ni, A. K. Y. Jen, C. S. Lee, Y. Chi, *Adv. Funct. Mater.* **2019**, *30*.

[23]. T. C. Lee, J. Y. Hung, Y. Chi, Y. M. Cheng, G. H. Lee, P. T. Chou, C. C. Chen, C. H. Chang, C. C. Wu, *Adv. Funct. Mater.* **2009**, *19*, 2639-2647.

[24]. C. You, D. Liu, J. Yu, H. Tan, M. Zhu, B. Zhang, Y. Liu, Y. Wang, W. Zhu, *Adv. Opt. Mater.* **2020**, *8*, 2000154.

[25]. C. You, D. Liu, L. Wang, W. Zheng, M. Li, P. Wang, W. Zhu, *Chem. Eng. J.* **2023**, *452*, 138956.

[26]. J. Xue, L. Xin, J. Hou, L. Duan, R. Wang, Y. Wei, J. Qiao, *Chem. Mater.* **2017**, *29*, 4775-4782.

[27]. L. K. Li, M. C. Tang, W. L. Cheung, S. L. Lai, M. Ng, C. K. M. Chan, M. Y. Chan, V. W. W. Yam, *Chem. Mater.* **2019**, *31*, 6706-6714.

[28]. J. X. Chen, Y. F. Xiao, K. Wang, D. Sun, X. C. Fan, X. Zhang, M. Zhang, Y. Z. Shi, J. Yu, F. X. Geng, C. S. Lee, X. H. Zhang, *Angew. Chem. Int. Ed.* **2021**, *60*, 2478-2484.

[29]. Y. J. Yu, Y. Hu, S. Y. Yang, W. Luo, Y. Yuan, C. C. Peng, J. F. Liu, A. Khan, Z. Q. Jiang, L. S. Liao, *Angew. Chem. Int. Ed.* **2020**, *59*, 21578-21584.